PLOS ONE

RESEARCH ARTICLE

Comparing lifeact and phalloidin for super-resolution imaging of actin in fixed cells

Hanieh Mazloom-Farsibaf[1☯¤a], Farzin Farzam[1☯¤b], Mohamadreza Fazel[1¤c], Michael J. Wester[1,2], Marjolein B. M. Meddens[1¤d], Keith A. Lidke[1,3]*

1 Department of Physics and Astronomy, University of New Mexico, Albuquerque, New Mexico, United States of America, **2** Department of Mathematics and Statistics, University of New Mexico, Albuquerque, New Mexico, United States of America, **3** Comprehensive Cancer Center, University of New Mexico, Albuquerque, New Mexico, United States of America

☯ These authors contributed equally to this work.
¤a Current address: Lyda Hill Department of Bioinformatics, University of Texas Southwestern Medical Center, Dallas, Texas, United States of America
¤b Current address: RNA Therapeutics Institute, University of Massachusetts Medical School, Worcester, Massachusetts, United States of America
¤c Current address: Center for Biological Physics, Department of Physics, Arizona State University, Tempe, Arizona, United States of America
¤d Current address: Department of Radiology and Nuclear Medicine, University Medical Center Utrecht, The Netherlands
* klidke@unm.edu

Citation: Mazloom-Farsibaf H, Farzam F, Fazel M, Wester MJ, Meddens MBM, Lidke KA (2021) Comparing lifeact and phalloidin for super-resolution imaging of actin in fixed cells. PLoS ONE 16(1): e0246138. https://doi.org/10.1371/journal.pone.0246138

Editor: Thomas Abraham, Pennsylvania State Hershey College of Medicine, UNITED STATES

Received: August 28, 2020

Accepted: January 13, 2021

Published: January 28, 2021

Data Availability Statement: Collected raw data is available at: https://doi.org/10.5061/dryad.xsj3tx9cn

Funding: This work was supported by NIH grants R01GM109888, 1R21EB019589 and the New Mexico Spatiotemporal Modeling Center (NIH P50GM085273). We gratefully acknowledge the use of the University of New Mexico Comprehensive Cancer Center fluorescence microscopy core, as well as the NIH P30CA118100 support for these cores. A Rubicon grant from the

Abstract

Visualizing actin filaments in fixed cells is of great interest for a variety of topics in cell biology such as cell division, cell movement, and cell signaling. We investigated the possibility of replacing phalloidin, the standard reagent for super-resolution imaging of F-actin in fixed cells, with the actin binding peptide 'lifeact'. We compared the labels for use in single molecule based super-resolution microscopy, where AlexaFluor 647 labeled phalloidin was used in a dSTORM modality and Atto 655 labeled lifeact was used in a single molecule imaging, reversible binding modality. We found that imaging with lifeact had a comparable resolution in reconstructed images and provided several advantages over phalloidin including lower costs, the ability to image multiple regions of interest on a coverslip without degradation, simplified sequential super-resolution imaging, and more continuous labeling of thin filaments.

Introduction

Super-resolution methods are optical microscopy methods that surpass the diffraction limit of light, either by manipulating the illumination pattern like STED [1] and SSIM [2] or by stochastic single molecule techniques like (d)STORM [3, 4], (f)PALM [5, 6], and PAINT [7]. These methods can achieve resolution that is more than one order of magnitude better than the diffraction limit and provide a tool to investigate biological processes down to the single-molecule level. Equally important in the advancement of super-resolution imaging has been the development of new fluorescent probes. For the stochastic methods, the required

Netherlands Organization for Scientific Research (NWO Rubicon 825.14.020) supported M.B.M.M. R01GM109888 supported: Keith Lidke and Hanieh Mazloom-Farsibaf 1R21EB019589 supported: Keith Lidke and Mohamadreza Fazel P50GM085273 supported: Keith Lidke, Mohamadreza Fazel, and Michael Wester NWO Rubicon 825.14.020 supported: Marjolein Meddens P30CA118100 supported: Keith Lidke, Michael Wester The funders had no role in study design, data collection and analysis, decision to publish, or preparation of the manuscript.

Competing interests: The authors have declared that no competing interests exist.

intermittent fluorescence (blinking) can be from fluorophores that photo-activate, photo-switch between the on- and off-state or reversibly bind to the target protein. (d)STORM takes advantage of fluorophores that can rapidly switch between on- and off-states for single molecule localization. PAINT uses transient immobilization of fluorophores binding to a target structure in order to produce single point objects and localize fluorescent events [7]. More recently, DNA-PAINT combined the capabilities of PAINT with programmable DNA hybridization to enable a range of reversible binding mechanisms, leading to higher specificity in target detection as well as higher numbers of individual fluorophores [8, 9].

A common target in super-resolution is the actin cytoskeleton. Actin exists in cells as either free, monomeric globular actin (G-actin) or filamentous actin (F-actin) [10, 11]. The dynamic equilibrium between these states regulates actin filament assembly and disassembly, which in turn controls multiple cellular processes, from cell migration and division to transport of intracellular vesicles. Changes in the regulation of the actin cytoskeleton, whether by mutation of actin itself or actin binding proteins, is associated with a number of diseases [12, 13]. In addition to its biomedical importance, imaging of the actin cytoskeleton is a common benchmark for validation of super-resolution methods. A variety of fluorescent probes for imaging actin have been compared in both live and fixed cells [14, 15], including actin chromobodies [16], utrophin [17], f-tractin [18], silicon rhodamine (SiR)-actin [19], epitope-tagged actin [20], fluorescent protein-actin fusion proteins [21], Affirmers [22], phalloidin as an F-actin-binding reagent [23], and lifeact [24]. In this work, we focus on two actin-labeling reagents, phalloidin and lifeact.

Phalloidin is a heptapeptide derived from the poisonous mushroom *Amanita phalloides* that binds with high specificity to F-actin and prevents filament depolymerization [25, 26]. Direct conjugation of fluorophores to phalloidin makes it a convenient tool for labeling of filamentous actin. However, the dissociation rate of phalloidin is approximately 10^{-4} 1/s [27], leading to some loss of label from dissociation during the ~ 1 hour imaging time. Phalloidin is typically limited to use in fixed cells due to the toxicity induced by its stabilization of the actin filaments and the fact that it is not membrane permeable [23, 28].

Lifeact is a short peptide taken from the first 17 amino acids of the yeast Abp140 and can be expressed in cells linked to a fluorescent protein to visualize F-actin dynamics [24]. Lifeact exchanges rapidly on F-actin with a dissociation rate less than one second [24, 29]. The peptide is small enough that it can be directly synthesized and a milligram amount provides an effectively inexhaustible supply for a typical lab when used for single-molecule imaging. Lifeact has been employed for super-resolution imaging of the actin filaments for a wide range of applications in live cells [30] and in fixed cells [29].

In this article, we compare the quality of lifeact in single molecule super-resolution imaging to phalloidin labeling. To image phalloidin, we used the dSTORM technique [4] where phalloidin was conjugated to AlexaFluor 647 (AF647), a spontaneously photo-switching dye for single-molecule super-resolution imaging [31]. For lifeact, we used the bright, photostable dye Atto 655 and lifeact's spontaneous binding and unbinding to actin to produce single molecule localizations similar to the (DNA)-PAINT approaches [29]. We compared lifeact with phalloidin labeling using several metrics including the average resolution of the reconstructed image, apparent filament thickness and continuity, data collection from multiple regions on a coverslip, and for use in sequential super-resolution imaging.

Materials and methods

Cell culture and reagents

HeLa and RBL-2H3 cells were originally purchased from ATCC. HeLa cells were authenticated by short-tandem repeat analysis. RBL-2H3 cells are routinely checked for binding of IgE and

the ability of the cells to degranulate. HeLa cells were cultured in Dulbecco's Modified Eagle Medium (Life Technologies, Cat No. 10313-v021) supplemented with 10% cosmic calf serum (HyClone), 5U/ml penicillin, 0.05 mg/ml streptomycin, and 2 mM L-glutamine (ThermoFisher, Cat No. 25030081) and maintained at 37 ˚C and 5% carbon dioxide. Rat Basophilic Leukemia (RBL-2H3) cells were cultured in MEM supplemented with 10% heat-inactivated fetal bovine serum, 5 U/ml penicillin, 0.05 mg/ml streptomycin, and 2mM L-glutamine at 37 ˚C and 5% carbon dioxide. For imaging, cells were plated overnight on 25 mm coverslips (1.5, Warner Instruments, #CS-25R15).

Cell fixation and actin labeling

Samples were fixed using a cytoskeleton-preserving buffer composed of 80 mM Pipes, 5 mM EGTA, and 2 mM $MgCl_2$ (PEM) with pH 7.2. Briefly, cells were washed with warm PEM and fixed in 0.6% paraformaldehyde with 0.1% glutaraldehyde and 0.25% Triton diluted in PEM buffer for 60 seconds and followed by a hard fixative buffer including 4% paraformaldehyde and 0.2% glutaraldehyde diluted in PEM for two hours. Cells were washed 2x in PBS, incubated for 10 min in 0.1% $NaBH_4$ for 10 min to reduce background fluorescence due to glutaraldehyde, and followed by a 2x wash with PBS. To quench reactive cross-linkers, the samples were incubated in 10 mM Tris for 10 min, followed by 2 washes with PBS. Finally, samples were permeabilized by incubation for 15 min in 5% BSA and 0.05% Triton X-100 diluted in PBS. At the end, samples were washed 1x with PBS and prepared for the labeling process.

To label actin using phalloidin, fixed cells were incubated for an hour in 0.56 μM AF647-conjugated to phalloidin (ThermoFisher, Cat no. A22287) in PBS. The samples were washed once in PBS and placed in dSTORM imaging buffer. The dSTORM buffer included an enzymatic oxygen scavenging system and primary thiol: 50 mM tris, 10 mM NaCl, 10% w/v glucose, 168.8 U/ml glucose oxidase (Sigma, Cat No. G2133), 1404 U/ml catalase (Sigma, Cat No. C9322), and 60 mM 2-aminoethanethiol (MEA) (Sigma-Aldrich, Cat no. M6500-25G) with pH 8.0, to provide a suitable chemical condition for having a photo-switchable AF647 dye.

For lifeact labeling, we used a customized 17-amino-acid peptide conjugated to Atto 655, (sequence: [Atto 655] CMGVADLIKKFESISKEE[COOH] (Bio-Synthesis, Lot No. P5869-1)). For imaging, lifeact was diluted to 0.7 nM in an optimized imaging buffer including 10 mM HEPES, 150 mM NaCl, 10% glucose, and 0.1% BSA with pH 7.0 for labeling the actin filaments.

25 mm coverslips were mounted in an Attofluor cell chamber (Life Technologies, Cat No. A-7816). The corresponding imaging buffer for each approach was added and a clean 25 mm coverslip was used to seal the chamber to avoid oxygen permeation into the buffer.

Sequential imaging

Sequential super-resolution was performed in a manner similar to that described by Valley *et a*l. [32]. First, actin structures were imaged using either phalloidin-AF647 or lifeact-Atto655. To remove the phalloidin signal, the sample was washed 4x with PBS before exposure to high intensity 638 nm laser light (~ 4.7 kW/cm^2) for 5 min to photobleach the sample, followed by a 20 min incubation in 0.1% $NaBH_4$ to quench any remaining active AF647 and finally washed 2x with PBS. To remove lifeact-Atto655, the sample was washed 12 x 1 min with 1 mM HEPES, 150 mM NaCl, 5% glucose, and 0.1% BSA in diH2O. In both cases, the sample was re-labeled with anti-α-tubulin-AF647 at 2.5 μg/ml for an hour in 2% BSA, 0.05% Triton diluted in PBS, followed by 3x wash with 2% BSA and 0.05% Triton in PBS for 5 min each. For data collection, the samples were kept in dSTORM buffer and sealed with a 25 mm coverslip. Re-alignment of the sample was done using a brightfield reference image as described by Valley *et a*l. [32].

Optical setup

The samples were mounted on the stage of a microscope with a custom-designed chamber holder. The imaging system was built on an inverted microscope (IX71, Olympus America Inc.). A nano positioning stage (Mad City Labs, Nano-LPS100) mounted on an *x-y* manual stage was installed on the microscope for cell location and brightfield registration. A mounted LED with a wavelength of 850 nm (M850L3, Thorlabs) was used for brightfield illumination. Brightfield images were collected on a CMOS camera (Thorlabs, DCC1545M) after reflection by a short-pass dichroic beam splitter (Semrock, FF750-SDi02) and then passing through a single-band bandpass filter (Semrock, FF01-835/70-25). A 638 nm laser (Thorlabs, L638P200) was coupled into a single-mode fiber and reflected by a dichroic beam splitter (Semrock, Di03-R635-t1-25x36) then focused onto the back focal plane of the 1.49 NA objective lens (UAPON 100XOTIRF, Olympus America Inc.). Emission for super-resolution data was collected through a short-pass dichroic beam splitter (Semrock, FF750-SDi02) and a single-band bandpass filter (Semrock, FF624-Di01) on an EMCCD camera (Andor Technologies, iXon DU-860E-CS0-#BV). All the instruments were controlled by custom-written software in MATLAB (MathWorks Inc.) [33]. Imaging was performed with a 638 nm laser at ~ 4.7 kW/cm^2 in TIRF (total internal reflection fluorescence) illumination with an approximate exposure time of 40 ms for lifeact and 10 ms for phalloidin (see Exposure time optimization). Brightfield registration was employed to correct for drift after every 3000 frames for phalloidin experiments and 2000 frames for lifeact experiments, as described in [34].

Data analysis

All analyses were performed using a custom-written single molecule analysis (SMA) software package in MATLAB combined with the Statistics Toolbox (The MathWorks, Inc) and DIPimage [35]. For 2D raw data, single emitters in each frame were identified as single localized spots. The parameters of each emitter, which includes positions, total photon count, background photon counts and their standard errors were computed by maximum likelihood estimation on a GPU [36]. After applying a threshold on maximum background photon counts of 200, minimum photon counts per frame per emitter of 250, and a data-model hypothesis test [37] with a cutoff p-value at 0.01, a well-defined set of localizations was reconstructed to generate a super-resolution image. To eliminate outliers, a nearest neighbor filter was employed to remove those localizations having less than 2 (1) neighbors within 15 nm for the lifeact (phalloidin) approach (see S1 Fig).

Fourier Ring Correlation (FRC) analysis

To estimate the resolution from the super-resolution images of phalloidin and lifeact, we used Fourier Ring Correlation (FRC) [38], which measures the average resolution over a single super-resolution image. In this method, the localized single emitters of a super-resolution image are divided into two statistically independent subsets. The image resolution is defined as the inverse of the spatial frequency when the FRC curve drops below a threshold of 1/7. Spurious correlations were removed by estimating the number of times an emitter was localized on average (Q) assuming Poisson statistics. All analyses were accomplished using the MATLAB software developed by Nieuwenhuizen *et al*. [38] found at http://www.diplib.org/add-ons.

Exposure time optimization

To acquire optimized super-resolution data, the camera exposure times were adjusted to be the same as the average blinking on-time, which for lifeact is the average time the peptide stays

bound to actin before dissociation. The on-time periods have an exponential distribution with an average of $1/k_{off}$, where k_{off} is the rate of emitters going from on to off in units of 1/ms (S2 Fig). To estimate the average on-time of blinking events in the lifeact approach, data sets were collected at various exposure times. Localizations from the same blinking events were connected across consecutive frames and this total time was used to create histograms for analysis. The on-time histogram was fit to an exponential distribution using a Poisson noise model by maximizing the likelihood given by

$$L(k_{off}|N, b, c) = \frac{(Nk_{off}e^{-Kb})^c e^{-(Nk_{off}e^{-Kb})}}{c!}$$

where b, c and N, respectively, stand for the number of localizations per binding event, the frequency of blinking events with a specific number of connected localizations, and the total number of localizations. The average on-time of the blinking events is then given by $\tau = \Delta T/k_{off}$, where ΔT is the exposure time for data acquisition.

Thickness and continuity assessment of actin filaments in reconstructed images

To evaluate the thickness and continuity of actin filaments in reconstructed images, regions of interest (ROIs) containing a segment of filament were selected manually. The selected segments were rotated to be along the x-axis to facilitate subsequent comparisons. The aligned actin segments were used to find the sum of normalized intensity distributions along and perpendicular to the x-axis to assess the continuity and thickness of the actin filaments, respectively. The resulting intensity distributions perpendicular to the x-axis shows the cross section of actin filaments, and their widths at half maximum were reported as actin thicknesses. A metric for continuity, which we call the continuity percentage, was calculated from the normalized intensity as the percent of the filament where the intensity along the length of the filament in the super-resolution image was greater than 25%.

Results

Resolution in super-resolution images

We employed the two actin labeling approaches using phalloidin and lifeact and compared the super-resolution images of actin structures in fixed HeLa and RBL-2H3 cells. The reversible binding of lifeact generates a small percentage of spurious localizations from transient, non-specific binding. These appear as isolated localizations away from any filaments. Localizations that did not have at least four other localizations within 15 nm were removed before further analysis (see Methods, S1 Fig). To evaluate the resolution in each imaging condition, we used Q-corrected Fourier Ring Correlation (FRC), which measures the average resolution over a single super-resolution image [38]. Actin filaments of HeLa cells are shown in Fig 1A and 1B. The FRC resolution measurements for the lifeact and phalloidin images ranged from 52.7 nm to 60.5 nm, and 52.4 nm to 58.7 nm, respectively. We repeated the same scenario for RBL-2H3 cells (Fig 1C and 1D) and obtained average resolutions ranging from 49.5 nm to 59.2 nm, and 36.3 nm to 45.1 nm for lifeact and phalloidin, respectively. The FRC curve estimates the average resolution of a super-resolution image as the inverse of the spatial frequency when the curve crosses the 1/7 line (Fig 2, red line, see also Methods). As depicted in Fig 2A (2B) for three HeLa (RBL-2H3) cells from different samples, phalloidin produced an equal or slightly improved average resolution compared to the lifeact.

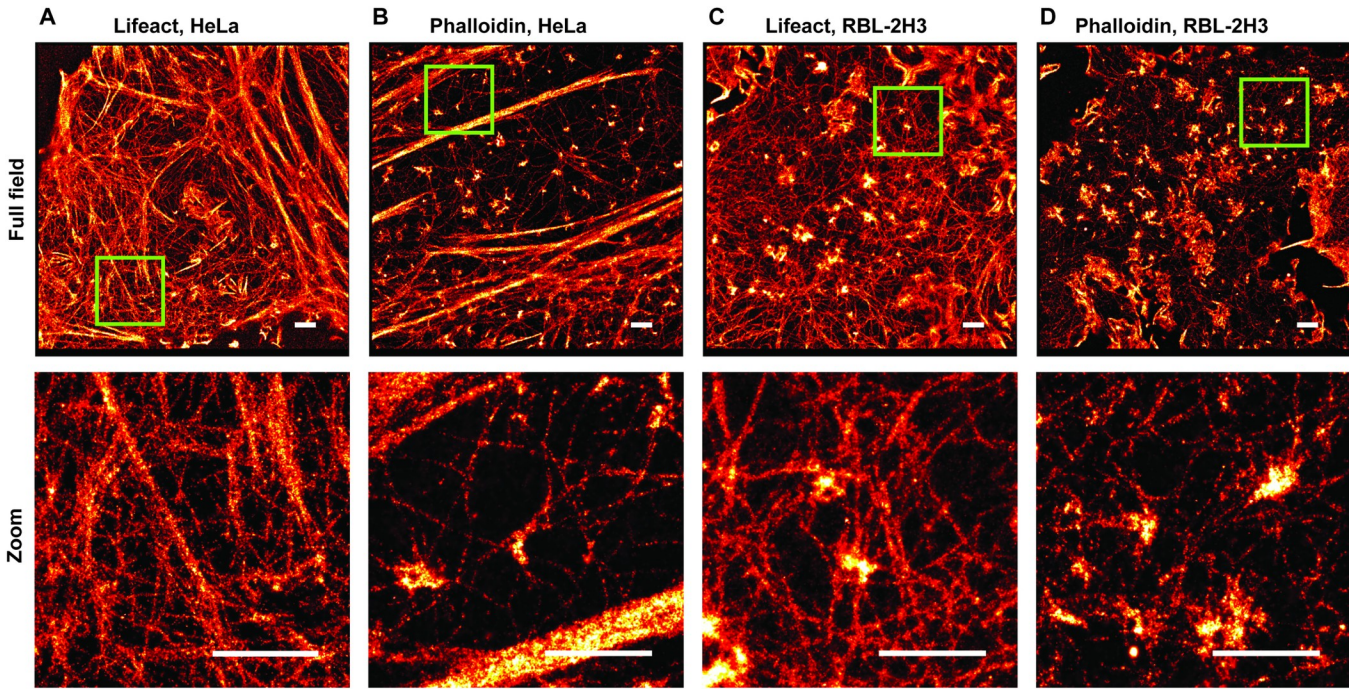

Fig 1. Super-resolution images of F-actin. (A) F-actin labeled with lifeact-Atto655 in a Hela cell image (top), zoomed-in image (bottom). (B) F-actin labeled with phalloidin-AF647 in a Hela cell (top), zoomed-in image (bottom). (C) F-actin labeled with lifeact-Atto655 in a RBL-2H3 cell image (top), zoomed-in image (bottom). (D) F-actin labeled with phalloidin-AF647 in a RBL-2H3 cell image (top), zoomed-in image (bottom). Scale bars, 1 μm.

https://doi.org/10.1371/journal.pone.0246138.g001

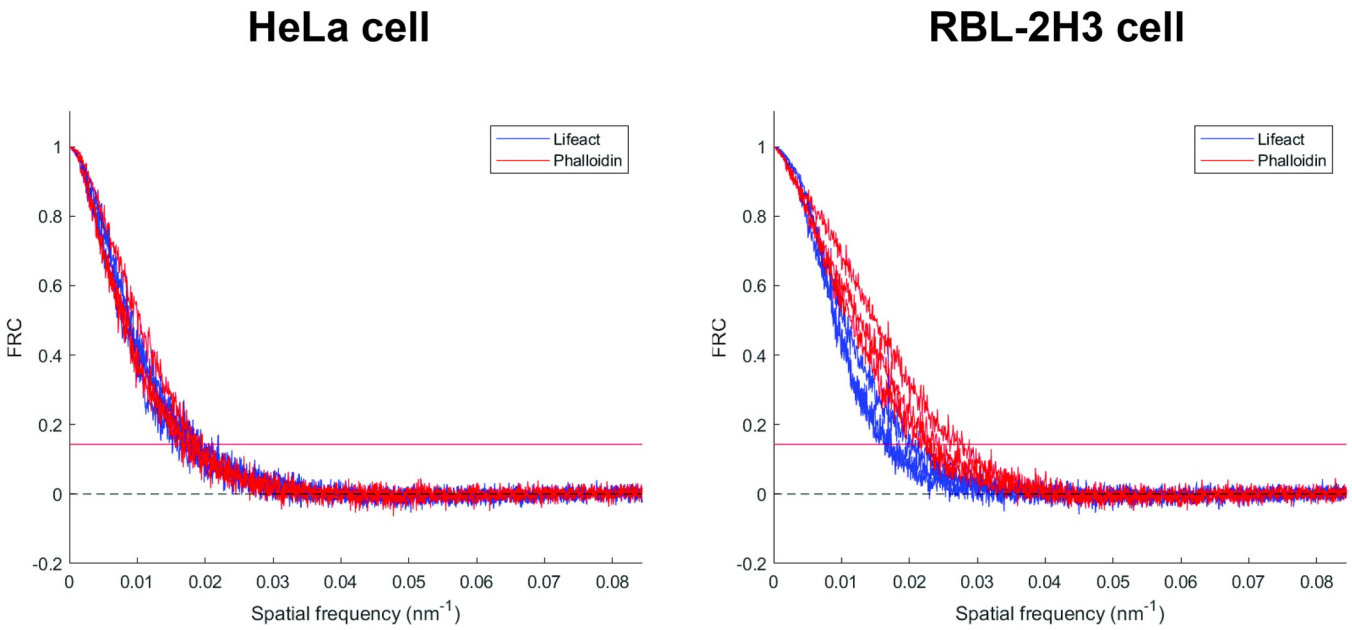

Fig 2. FRC curves for super-resolution images of F-actin. (Left) FRC curve of F-actin super-resolution images in HeLa cells from three samples of independent experiments for lifeact (blue) and phalloidin (red). (Right) FRC curves of F-actin super-resolution images in RBL-2H3 cells from three samples of independent experiments for lifeact (blue) and phalloidin (red). The horizontal red line at FRC = 1/7 indicates the value of the average resolution, which is defined as the inverse of the spatial frequency at this point.

https://doi.org/10.1371/journal.pone.0246138.g002

Filament thickness and continuity

We estimated the thickness and continuity of actin filaments found in images from each condition. As illustrated in Fig 3 with small green boxes, several thin filaments were manually selected from the reconstructed super-resolution image for lifeact (Fig 3A) and phalloidin (Fig 3B). For each condition, we chose two super-resolution imaging results (S3 Fig) and selected 22 filaments in each condition. The reconstructed thickness was found to be approximately 30 (36) nm at FWHM (Full Width at Half Maximum) of cross-sectional profile for individual filaments in lifeact (phalloidin) approach (see Methods, Fig 3C). To evaluate the continuity of observed actin filaments for each strategy, the normalized intensity along thin filaments is shown in Fig 3D (top (lifeact), bottom (phalloidin)). We calculated the continuity of single filament above the 25% of normalized intensity. The median (mean) of the continuity percentage (see Methods) of single filaments was 98.1% (93.4%) for lifeact versus 91.4% (90.3%) for

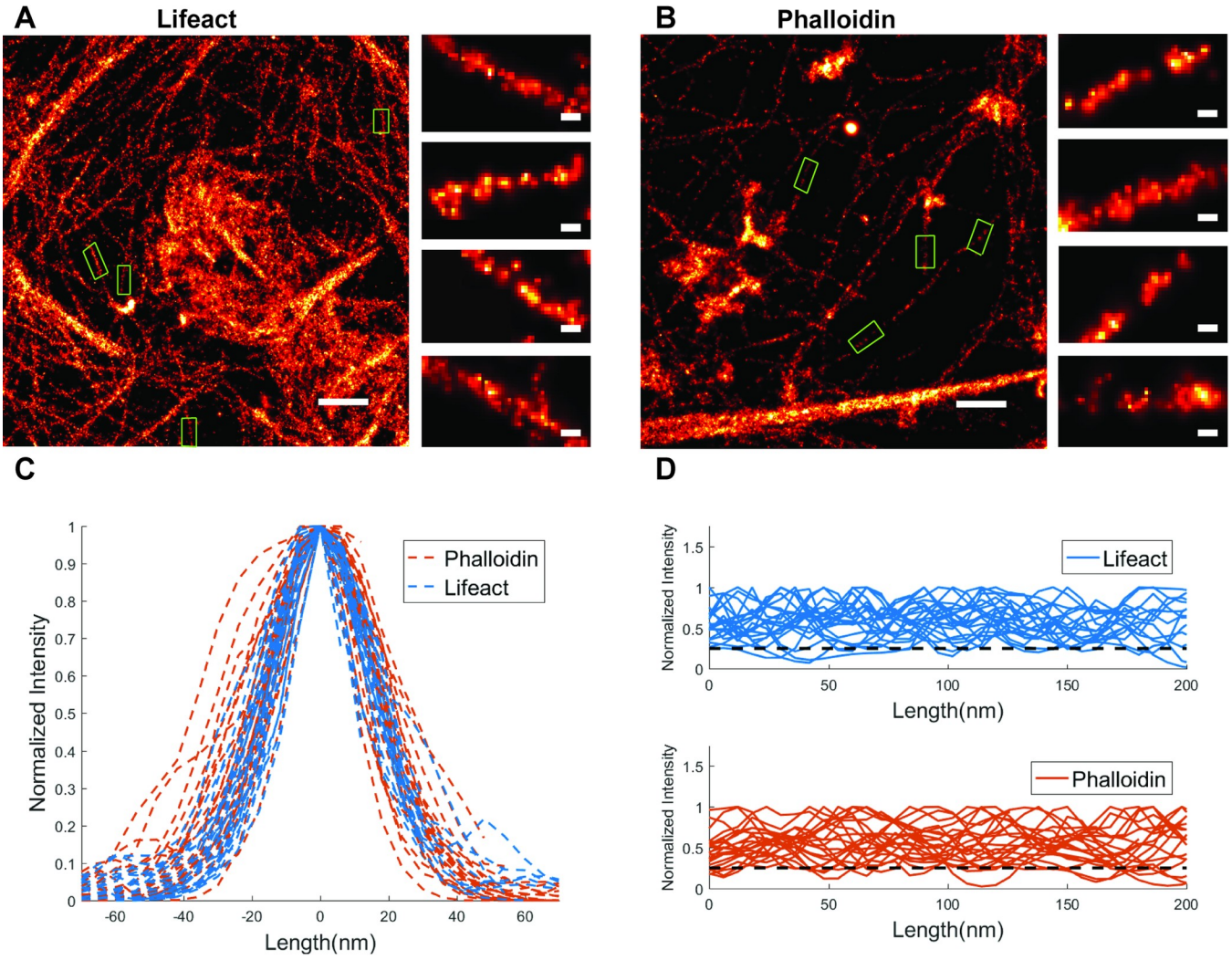

Fig 3. Comparison of lifeact and phalloidin for individual actin filaments. (A) Super-resolution image from lifeact tagged sample. (B) Super-resolution image from phalloidin tagged sample. The green boxes show several selected filaments. (C) The normalized intensities of the selected filaments through the filament cross-section. (D) The normalized intensities along the selected filaments, for the lifeact (top) and phalloidin (bottom) methods. Dashed line is the 25% of the normalized intensity. The scale bars in full field images are 500 nm. The scale bars in zoomed regions are 30 nm.

https://doi.org/10.1371/journal.pone.0246138.g003

phalloidin. A comparison of the number of localizations obtained on a single actin filament over time with either lifeact and phalloidin is shown in (S4 Fig).

Multiple dataset collection

It is often desired to collect data from multiple cells or regions on one coverslip. To investigate this aspect, we imaged actin structures for an extended period using both labeling methods. We found that the lifeact approach provided a near constant number of localizations per frame, whereas the number of localizations per frame with phalloidin imaging dropped considerably even during the imaging of the first cell on a coverslip (S5 Fig). This can be explained by reversible binding of lifeact from a large pool of lifeact in the imaging buffer whereas phalloidin suffers from both photobleaching and dissociation over the timescale of hours. Fig 4 depicts the reconstructed super-resolution image for the lifeact approach where imaging began after 10 min (Fig 4A) or 17 hr (Fig 4B) of adding the imaging buffer. We also collected data with the phalloidin approach with imaging starting after 5 min (Fig 4C) or 2 hr (Fig 4D) of adding the imaging buffer. Lifeact imaging showed no decrease in performance for the later data collection while phalloidin suffered from reduced phalloidin labeling due to dissociation before the start of imaging.

Sequential imaging

Imaging of multiple structures within the same cell is of interest in order to reveal a spatial correlation between the cellular structures. Here, we compared phalloidin and lifeact strategies in

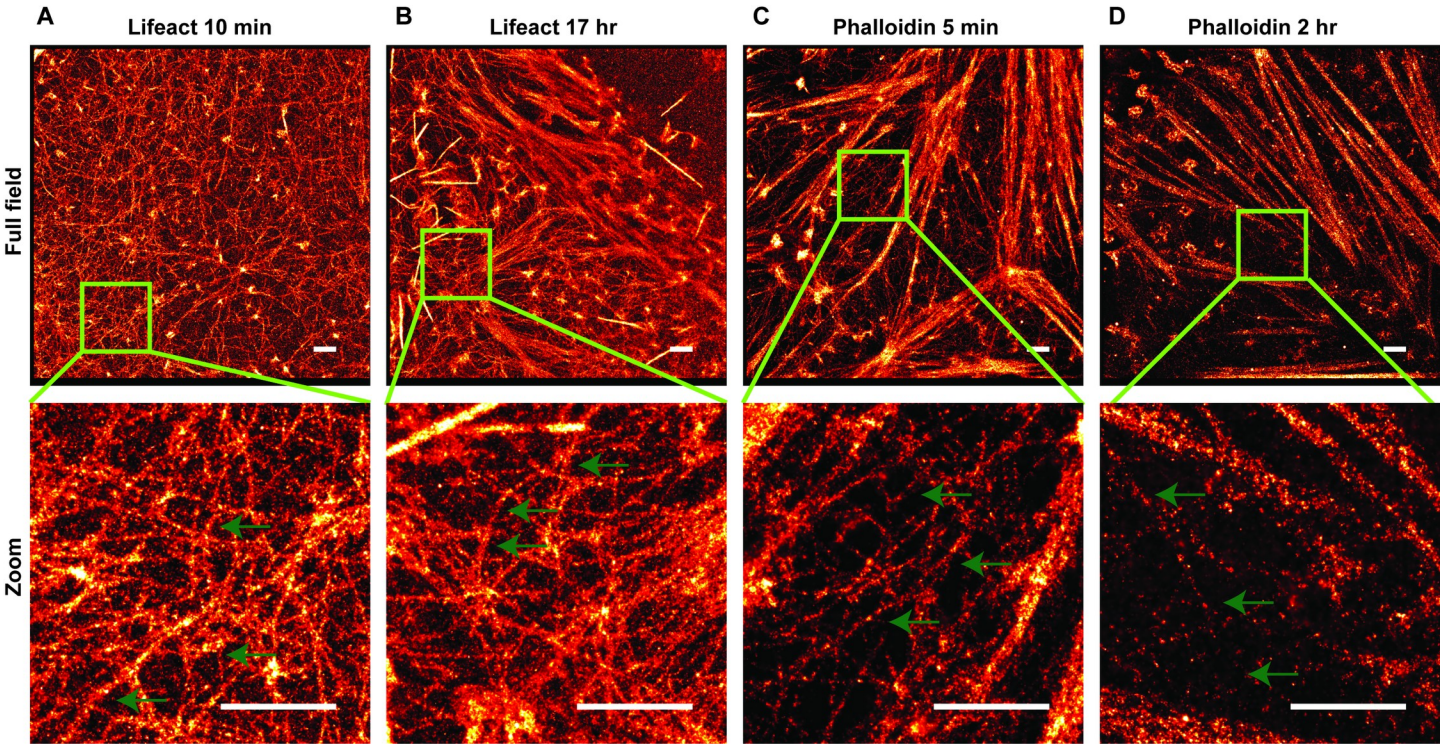

Fig 4. Super-resolution of actin filaments in HeLa cells at various time-points after the start of imaging. (A) Super-resolution of F-actin labeled with lifeact-Atto655 in the full field image (top) and the zoomed-in image (bottom); data collection was started at 10 min after adding the imaging buffer; (B) Super-resolution of F-actin labeled with lifeact-Atto655 in the full field image (top) and the zoomed-in image (bottom); data collection was started at 17 hr after adding the imaging buffer. (C) Super-resolution of F-actin labeled with phalloidin-AF647 in the full field image (top) and the zoomed-in image (bottom); data was collected after adding the imaging buffer within 5 min. (D) Super-resolution of F-actin labeled with phalloidin-AF647 in the full field image (top) and the zoomed-in image (bottom); data was collected after adding the imaging buffer within 2 hr. The green arrows point to some thin filaments to show their continuities. The scale bar is 1 μm.

https://doi.org/10.1371/journal.pone.0246138.g004

their capacity for sequential super-resolution imaging [32]. As depicted in Fig 5A, the first round of labeling was to detect actin using lifeact or phalloidin. After removal of the actin-binding probe (see Methods), microtubules were imaged with dSTORM in the same samples (Fig 5B). The green boxes in Fig 5A showcase bright actin bundles, where abundance of actin-binding markers were detected before being removed completely for the second round of imaging on microtubules (Fig 5B). Fig 5C shows the overlay of actin filaments and microtubules in the subregions indicated in Fig 5B.

Discussion

In evaluating super-resolution imaging results of the lifeact and phalloidin labeling methods, we considered four aspects: image resolution, filament thickness and continuity, multiple data-set collection, and capability for sequential imaging. The resolution as measured by FRC analysis showed that the average resolution in the case of lifeact is comparable or to that with phalloidin, with phalloidin having a small advantage in the RBL cells but not in the HeLa cells. It is important to note that the FRC resolution measure gives an average resolution over the image, but cannot directly assess the quality of labeling.

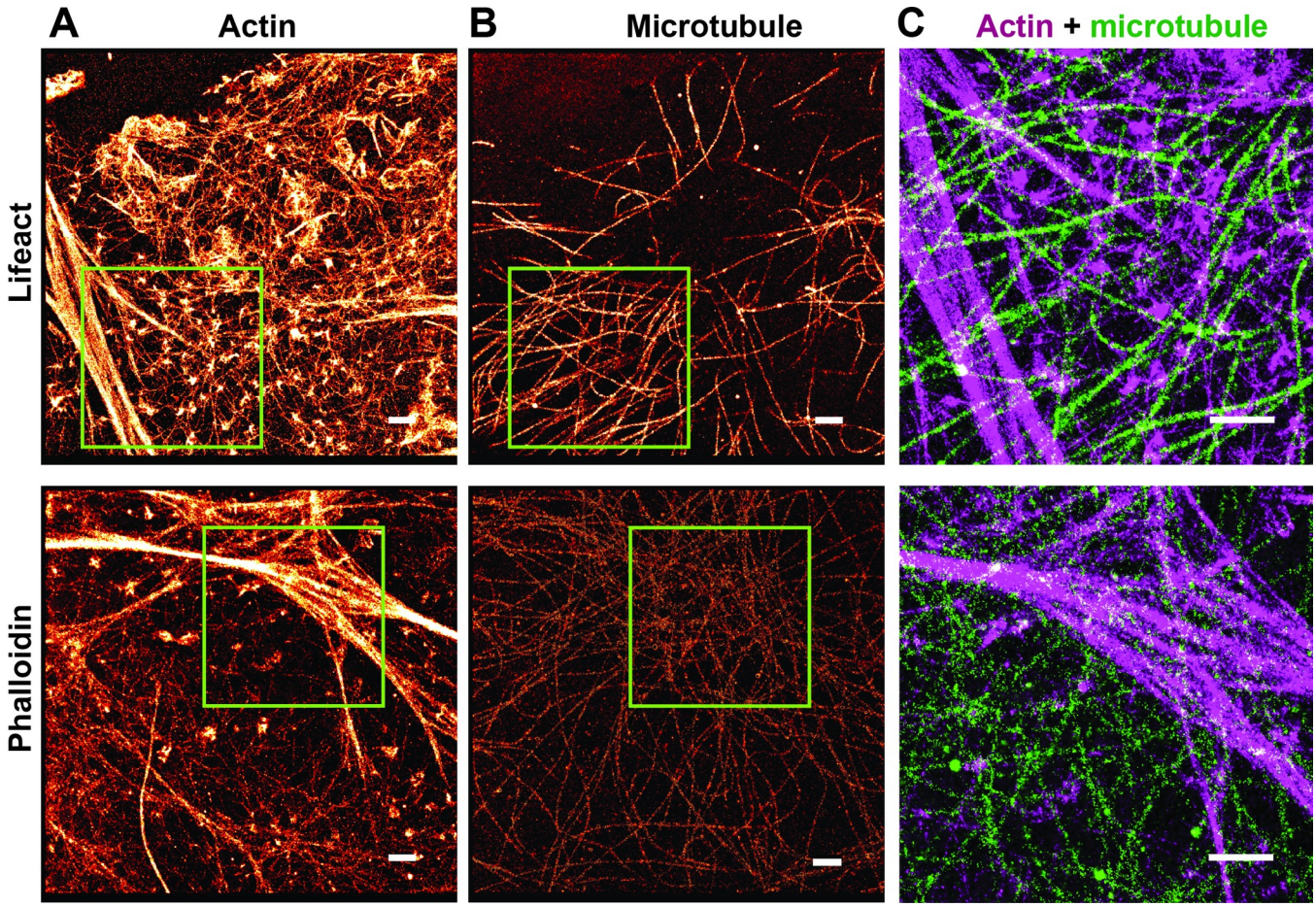

Fig 5. Sequential imaging of actin structures and microtubules in HeLa cells. (A) Super-resolution image of F-actin labeled with lifeact-Atto655 (top) and phalloidin-AF647 (bottom). (B) Super-resolution image of microtubules of the same cell. (C) Overlay of actin structures (red) and microtubules (green) from the subregion selected by the green box when lifeact (top) or phalloidin (bottom) were used for actin imaging. The scale bar is 1 μm.

https://doi.org/10.1371/journal.pone.0246138.g005

Targeting the actin binding sites depends on the biochemical structure of each actin-detecting probe and the various actin architectures [15]. For example, lifeact fails to detect some fine structures such as filopodia in mesenchymal cells [39] or cofilin-bound actin in STHdh cells [40] whereas phalloidin does not bind to filaments with less than seven actin subunits [41]. We evaluated the labeling quality by individual filaments analysis (thickness and continuity) in the reconstructed super-resolution images. This analysis reported an average apparent thickness of 30 nm for lifeact approach versus 36 nm for phalloidin, and suggested the continuity of actin filaments is slightly greater in the lifeact method. For actin bundles where the number of binding sites are much higher than for single filaments, the reconstructed super-resolution images appear as bright regions in both methods; however, for single filaments, the lifeact method results in a somewhat more continuous visualization of the actin filaments.

The blinking mechanism in the lifeact method depends on the binding/unbinding of the peptide. This process benefits from a bright, photostable dye, such as Atto655 so that it doesn't photobleach as it diffuses into the TIRF field, binds actin, is imaged for ~ 0.1 s, and then unbinds a diffuses away. The large pool of dye-labeled lifeact provides for consistent localizations over long imaging periods as the probes are replenished from the buffer pool. However, the background fluorescence from the fluorescent, diffusing lifeact requires a TIRF or near-TIRF modality to reduce background, restricting imaging to near the coverslip. Phalloidin is semi-permanently bound to actin with a dissociation rate of a few hours. In this case, the blinking mechanism is provided by light-activated photoswitching of the AF647 label. Because the label is not replenished, it invebitaly either undergoes photobleaching during data collection [31] or is lost from the dissociation of phalloidin. With lifeact, super-resolution images collected several hours after adding the imaging buffer showed no degradation of labeling, enabling multiple data sets to be collected from one coverslip. With phalloidin, the best image quality was always achieved from the first region imaged, with imaging performed just after washing out the free label. Subsequent regions suffered from reduced labeling from the phalloidin dissociation that occurred while imaging earlier regions.

Both methods were successful with the use of sequential labeling to image actin and microtubules within the same cell. Lifeact had the advantage that the probe could simply be washed out before microtubule labeling. After imaging phalloidin, the additional steps of photobleaching and quenching were required to eliminate crosstalk with the first imaging cycle.

In summary, we found that lifeact provides a reliable and inexpensive alternative to phalloidin for actin visualization in fixed cells, particularly for super-resolution imaging near the coverslip. Imaging with lifeact additionally confers several advantages over phalloidin including more continuous labeling of filaments, the ability to image multiple cells per sample and simplification of sequential super-resolution imaging.

Supporting information

S1 Fig. Nearest neighbor filtering to remove nonspecific localizations. (A) Reconstructed super-resolution images of actin filaments in HeLa cells labeled with lifeact-Atto655 (top) and phalloidin-AF647 (bottom). (B) Super-resolution images of actin filaments in HeLa cells labeled with lifeact-Atto655 (top) and phalloidin-AF647 (bottom) after removing localizations that had less than 4 other localizations within 15 nm. Scale bars are 500 nm.
(TIF)

S2 Fig. Estimation of average binding time for lifeact-Atto655. Data was collected with six exposure times: 25 ms, 30 ms, 33 ms, 35 ms, 38 ms, and 45 ms. The distribution of the number of connected localizations per binding event (blue) fits with an exponential model (red dashed line) to extract a binding lifetime.
(TIF)

S3 Fig. Super-resolution images of actin filaments in HeLa cells. (A) Super-resolution images from two lifeact tagged samples. (B) Super-resolution image from two phalloidin tagged samples. The scale bars in full field images are 500 nm.
(TIF)

S4 Fig. Cumulative number of localizations in actin filaments. Single filaments were cropped from the reconstructed super-resolution images from lifeact-Atto655 (top) and phalloidin-AF647 (bottom). The filaments were reconstructed using localizations from the first (A) 30,000, (B) 60,000 and (C) 100,000 frames. The scale bars are 20 nm. (D) The cumulative number of localizations per frame from data collected using lifeact (red) and phalloidin (blue). Data is from HeLa cells.
(TIF)

S5 Fig. Localizations per frame. Plots show the number of localized single molecules per frame for complete data collections for individual cells. (A) HeLa cells labeled with lifeact-Atto655. (B) RBL-2H3 cells labeled with lifeact-Atto655. (C) HeLa cells labeled with phalloidin-AF647. (D) RBL-2H3 cells labeled with phalloidin-AF647.
(TIF)

Acknowledgments

We thank Shayna Lucero for assistance with cell culture and Diane Lidke for suggestions on the manuscript.

Author Contributions

Conceptualization: Hanieh Mazloom-Farsibaf, Farzin Farzam, Marjolein B. M. Meddens, Keith A. Lidke.

Formal analysis: Hanieh Mazloom-Farsibaf, Mohamadreza Fazel.

Investigation: Hanieh Mazloom-Farsibaf, Farzin Farzam.

Project administration: Hanieh Mazloom-Farsibaf, Farzin Farzam.

Resources: Michael J. Wester.

Software: Mohamadreza Fazel, Michael J. Wester.

Supervision: Keith A. Lidke.

Visualization: Farzin Farzam.

Writing – original draft: Hanieh Mazloom-Farsibaf, Farzin Farzam, Michael J. Wester.

Writing – review & editing: Hanieh Mazloom-Farsibaf, Farzin Farzam, Michael J. Wester, Marjolein B. M. Meddens, Keith A. Lidke.

References

1. Hell SW, Wichmann J (1994) Breaking the diffraction resolution limit by stimulated emission: stimulated-emission-depletion fluorescence microscopy. Optics letters, 19(11):780–782. https://doi.org/10.1364/ol.19.000780 PMID: 19844443
2. Gustafsson MGL (2005) Nonlinear structured-illumination microscopy: wide-field fluorescence imaging with theoretically unlimited resolution. Proceedings of the National Academy of Sciences of the United States of America, 102(37):13081–13086. https://doi.org/10.1073/pnas.0406877102 PMID: 16141335

3. Rust MJ, Bates M, Zhuang X (2006) Sub-diffraction-limit imaging by stochastic optical reconstruction microscopy (STORM). Nature methods, 3(10):793–795. https://doi.org/10.1038/nmeth929 PMID: 16896339

4. Heilemann M, Van De Linde S, Schüttpelz M, Kasper R, Seefeldt B, Mukherjee A, et al. (2008) Subdiffraction-resolution fluorescence imaging with conventional fluorescent probes. Angewandte Chemie, International Edition, 47(33):6172–6176. https://doi.org/10.1002/anie.200802376 PMID: 18646237

5. Betzig E, Patterson GH, Sougrat R, Lindwasser OW, Olenych S, Bonifacino JS, et al. (2006) Imaging intracellular fluorescent proteins at nanometer resolution. Science, 313(5793):1642–1645. https://doi.org/10.1126/science.1127344 PMID: 16902090

6. Hess ST, Girirajan TPK, Mason MD (2006) Ultra-high resolution imaging by fluorescence photoactivation localization microscopy. Biophysical journal, 91(11):4258–4272. https://doi.org/10.1529/biophysj.106.091116 PMID: 16980368

7. Sharonov A, Hochstrasser RM (2006) Wide-field subdiffraction imaging by accumulated binding of diffusing probes. Proceedings of the National Academy of Sciences of the United States of America, 103 (50):18911–18916. https://doi.org/10.1073/pnas.0609643104 PMID: 17142314

8. Jungmann R, Steinhauer C, Scheible M, Kuzyk A, Tinnefeld P, Simmel FC (2010) Single-molecule kinetics and super-resolution microscopy by fluorescence imaging of transient binding on DNA origami. Nano letters, 10(11):4756–4761. https://doi.org/10.1021/nl103427w PMID: 20957983

9. Jungmann R, Avendaño MS, Woehrstein JB, Dai M, Shih WM, Yin P (2014) Multiplexed 3D cellular super-resolution imaging with DNA-PAINT and Exchange-PAINT. Nature methods, 11(3):313–318. https://doi.org/10.1038/nmeth.2835 PMID: 24487583

10. Pollard TD, Cooper JA (2009) Actin, a central player in cell shape and movement. Science, 326 (5957):1208–1212. https://doi.org/10.1126/science.1175862 PMID: 19965462

11. Dominguez R, Holmes KC (2011) Actin structure and function. Annual review of biophysics, 40:169–186. https://doi.org/10.1146/annurev-biophys-042910-155359 PMID: 21314430

12. Wickramarachchi DC, Theofilopoulos AN, Kono DH (2010) Immune pathology associated with altered actin cytoskeleton regulation. Autoimmunity, 43(1):64–75. https://doi.org/10.3109/08916930903374634 PMID: 20001423

13. Muñoz-Lasso DC, Romá-Mateo C, Pallardó FV, Gonzalez-Cabo P (2020) Much More Than a Scaffold: Cytoskeletal Proteins in Neurological Disorders. Cells, 9(2)https://doi.org/10.3390/cells9020358 PMID: 32033020

14. Spracklen AJ, Fagan TN, Lovander KE, Tootle TL (2014) The pros and cons of common actin labeling tools for visualizing actin dynamics during Drosophila oogenesis. Developmental biology, 393(2):209–226. https://doi.org/10.1016/j.ydbio.2014.06.022 PMID: 24995797

15. Melak M, Plessner M, Grosse R (2017) Correction: Actin visualization at a glance. Journal of cell science, 130(9):1688. https://doi.org/10.1242/jcs.204487 PMID: 28461556

16. Rocchetti A, Hawes C, Kriechbaumer V (2014) Fluorescent labelling of the actin cytoskeleton in plants using a cameloid antibody. Plant methods, 10:12. https://doi.org/10.1186/1746-4811-10-12 PMID: 24872838

17. Winder SJ, Hemmings L, Maciver SK, Bolton SJ, Tinsley JM, Davies KE, et al. (1995) Utrophin actin binding domain: analysis of actin binding and cellular targeting. Journal of cell science, 108 (Pt 1):63–71. PMID: 7738117

18. Schell MJ, Erneux C, Irvine RF (2001) Inositol 1,4,5-Trisphosphate 3-Kinase A Associates with F-actin and Dendritic Spines via Its N Terminus. The Journal of biological chemistry, 276(40):37537–37546. https://doi.org/10.1074/jbc.M104101200 PMID: 11468283

19. D'Este E, Kamin D, Göttfert F, El-Hady A, Hell SW (2015) STED nanoscopy reveals the ubiquity of subcortical cytoskeleton periodicity in living neurons. Cell reports, 10(8):1246–1251. https://doi.org/10.1016/j.celrep.2015.02.007 PMID: 25732815

20. Copeland JW, Treisman R (2002) The diaphanous-related formin mDia1 controls serum response factor activity through its effects on actin polymerization. Molecular biology of the cell, 13(11):4088–4099. https://doi.org/10.1091/mbc.02-06-0092 PMID: 12429848

21. Ballestrem C, Wehrle-Haller B, Imhof BA (1998) Actin dynamics in living mammalian cells. Journal of cell science, 111 (Pt 12):1649–1658. PMID: 9601095

22. Lopata A, Hughes R, Tiede C, Heissler SM, Sellers JR, Knight PJ, et al. (2018) Affimer proteins for F-actin: novel affinity reagents that label F-actin in live and fixed cells. Scientific reports, 8(1):6572. https://doi.org/10.1038/s41598-018-24953-4 PMID: 29700342

23. Wulf E, Deboben A, Bautz FA, Faulstich H, Wieland T (1979) Fluorescent phallotoxin, a tool for the visualization of cellular actin. Proceedings of the National Academy of Sciences of the United States of America, 76(9):4498–4502. https://doi.org/10.1073/pnas.76.9.4498 PMID: 291981

24. Riedl J, Crevenna AH, Kessenbrock K, Yu JH, Neukirchen D, Bista M, et al. (2008) Lifeact: a versatile marker to visualize F-actin. Nature methods, 5(7):605–607. https://doi.org/10.1038/nmeth.1220 PMID: 18536722

25. Wieland T, Faulstich H, Fiume L (1978) Amatoxins, Phallotoxins, Phallolysin, and Antamanide: The Biologically Active Components of Poisonous Amanita Mushroom. CRC critical reviews in biochemistry, 5 (3):185–260. https://doi.org/10.3109/10409237809149870 PMID: 363352

26. Cooper JA (1987) Effects of cytochalasin and phalloidin on actin. The Journal of cell biology, 105 (4):1473–1478. https://doi.org/10.1083/jcb.105.4.1473 PMID: 3312229

27. Cruz EMDL, De La Cruz EM, Pollard TD (1996) Kinetics and Thermodynamics of Phalloidin Binding to Actin Filaments from Three Divergent Species†. Biochemistry, 35(45):14054–14061. https://doi.org/10.1021/bi961047t PMID: 8916890

28. Yan Q, Schwartz SL, Maji S, Huang F (2014) Localization Microscopy using Noncovalent Fluorogen Activation by Genetically Encoded Fluorogen-Activating Proteins. https://onlinelibrary.wiley.com/doi/abs/10.1002/cphc.201300757

29. Kiuchi T, Higuchi M, Takamura A, Maruoka M, Watanabe N (2015) Multitarget super-resolution microscopy with high-density labeling by exchangeable probes. Nature Methods, 12(8):743–746. https://doi.org/10.1038/nmeth.3466 PMID: 26147917

30. Ashdown GW, Burn GL, Williamson DJ, Pandžić E, Peters R, Holden M, et al. (2017) Live-Cell Super-resolution Reveals F-Actin and Plasma Membrane Dynamics at the T Cell Synapse. Biophysical journal, 112(8):1703–1713. https://doi.org/10.1016/j.bpj.2017.01.038 PMID: 28445761

31. Dempsey GT, Vaughan JC, Chen KH, Bates M, Zhuang X (2011) Evaluation of fluorophores for optimal performance in localization-based super-resolution imaging. Nature methods, 8(12):1027–1036. https://doi.org/10.1038/nmeth.1768 PMID: 22056676

32. Valley CC, Liu S, Lidke DS, Lidke KA (2015) Sequential superresolution imaging of multiple targets using a single fluorophore. PloS one, 10(4):e0123941. https://doi.org/10.1371/journal.pone.0123941 PMID: 25860558

33. Pallikkuth S, Meddens M, Fazel M, Farsibaf H, Farzam F, Wester M, et al. (2018) A MATLAB-based Instrument Control Package for Fluorescence Imaging. Biophysical journal, 114(3):532a.

34. Wester MJ, Pallikkuth S, Mazloom-Farsibaf H, Fazel M, Schodt D, Lidke KA (2020) A Robust, Fiducial Free Drift Correction for Superresolution Imaging. Biophysical journal, 118(3):147a.

35. Hendriks CLL, Van Vliet LJ, Rieger B, Kempen GMP van, Ginkel M van (1999) DIPimage: a scientific image processing toolbox for MATLAB. Quantitative Imaging Group, Faculty of Applied Sciences, Delft University of Technology, Delft, The Netherlands,

36. Smith CS, Joseph N, Rieger B, Lidke KA (2010) Fast, single-molecule localization that achieves theoretically minimum uncertainty. Nature methods, 7(5):373–375. https://doi.org/10.1038/nmeth.1449 PMID: 20364146

37. Huang F, Schwartz SL, Byars JM, Lidke KA (2011) Simultaneous multiple-emitter fitting for single molecule super-resolution imaging. Biomedical optics express, 2(5):1377–1393. https://doi.org/10.1364/BOE.2.001377 PMID: 21559149

38. Nieuwenhuizen RPJ, Lidke KA, Bates M, Puig DL, Grünwald D, Stallinga S, et al. (2013) Measuring image resolution in optical nanoscopy. Nature methods, 10(6):557–562. https://doi.org/10.1038/nmeth.2448 PMID: 23624665

39. Sanders TA, Llagostera E, Barna M (2013) Specialized filopodia direct long-range transport of SHH during vertebrate tissue patterning. Nature, 497(7451):628–632. https://doi.org/10.1038/nature12157 PMID: 23624372

40. Munsie LN, Caron N, Desmond CR, Truant R (2009) Lifeact cannot visualize some forms of stress-induced twisted F-actin. Nature methods, 6(5):317. https://doi.org/10.1038/nmeth0509-317 PMID: 19404250

41. Kristó I, Bajusz I, Bajusz C, Borkúti P, Vilmos P (2016) Actin, actin-binding proteins, and actin-related proteins in the nucleus. Histochemistry and cell biology, 145(4):373–388. https://doi.org/10.1007/s00418-015-1400-9 PMID: 26847179